

# Growth of Linear Perturbations before the Era of the First Galaxies

S. Naoz and R. Barkana<sup>1</sup> <sup>★</sup>

<sup>1</sup>*School of Physics and Astronomy, The Raymond and Beverly Sackler Faculty of Exact Sciences, Tel Aviv University, Tel Aviv 69978, ISRAEL*

24 August 2021

## ABSTRACT

We calculate the evolution of linear density and temperature perturbations in a universe with dark matter, baryons, and radiation, from cosmic recombination until the epoch of the first galaxies. In addition to gravity, the perturbations are affected by electron scattering with the radiation, by radiation pressure, and by gas pressure. We include the effect of spatial fluctuations in the baryonic sound speed and show that they induce a  $\gtrsim 10\%$  change in the baryonic density power spectrum on small scales, and a larger change on all scales in the power spectrum of gas temperature fluctuations. A precise calculation of the growth of linear perturbations is essential since they provide the initial conditions for the formation of galaxies and they can also be probed directly via cosmological 21cm fluctuations. We also show that in general the thermal history of the cosmic gas can be measured from 21cm fluctuations using a small-scale anisotropic cutoff due to the thermal width of the 21cm line.

**Key words:** cosmology:theory – galaxies:formation – large-scale structure of universe

## 1 INTRODUCTION

Observations of the cosmic microwave background (CMB) show that the universe at cosmic recombination (redshift  $z \sim 10^3$ ) was remarkably uniform apart from spatial fluctuations in the energy density and in the gravitational potential of roughly one part in  $10^5$  (e.g., Bennett et al. 1996). The primordial inhomogeneities in the density distribution grew over time and eventually led to the formation of galaxies as well as galaxy clusters and large-scale structure.

Different physical processes contributed to the perturbation growth (e.g., Peebles 1980, 1993; Ma & Bertschinger 1995). In the absence of other influences, gravitational forces due to density perturbations imprinted by inflation would have driven parallel perturbation growth in the dark matter, baryons and photons. However, since the photon sound speed is of order the speed of light, the radiation pressure produced sound waves on a scale of order the horizon and suppressed sub-horizon perturbations in the photon density. The baryonic pressure similarly suppressed perturbations in the gas below the much smaller baryonic Jeans scale. Since the formation of hydrogen at recombination had decoupled the cosmic gas from its mechanical drag on the CMB, the baryons subsequently began to fall into the pre-existing gravitational potential wells of the dark matter.

Spatial fluctuations developed in the gas temperature as well as in the gas density. Both the baryons and the dark matter were affected on small scales by the temperature fluctuations through the gas pressure. Compton heating due to scattering of the residual free electrons (constituting a fraction  $\sim 10^{-4}$ ) with the CMB photons remained effective, keeping the gas temperature fluctuations tied to the photon temperature fluctuations, even for a time after recombination. In prior analyses (e.g., Peebles 1980; Ma & Bertschinger 1995) and in the standard CMBFAST code (Seljak & Zaldarriaga 1996) a spatially uniform speed of sound was assumed for the gas at each redshift. This assumption meant that the gas temperature distribution at any given time was assumed to be simply proportional to its density distribution. While this assumption can be accurately invoked before recombination, when the gas is thermally and mechanically coupled to the radiation, and in the absence of heating would be accurate after recombination (i.e., for an adiabatic gas), this assumption is in fact inaccurate during the post-recombination era due to the continual Compton heating. A full calculation of the temperature fluctuations is essential for obtaining accurate results for the small-scale density power spectra of both the baryons and (to a lesser degree) the dark matter (see also Yamamoto et al. (1997) and Yamamoto et al. (1998), who considered the effect of a varying sound speed on density perturbations). Note that whether we discuss perturbations driven by gravity or sound waves driven by pressure gradi-

<sup>★</sup> E-mail: smadar@wise.tau.ac.il (SN); barkana@wise.tau.ac.il (RB)

ents, we in every case refer to  $\delta p/\delta \rho$  as the square of the sound speed of the fluid, where  $\delta p$  and  $\delta \rho$  are the pressure and density perturbations, respectively.

The primordial inhomogeneities in the cosmic gas induced variations in the optical depth for absorption of the CMB at the redshifted 21cm wavelength of neutral hydrogen. Therefore, the hyperfine spin flip transition of neutral hydrogen is potentially the most promising tracer of the cosmic gas in the era before the first galaxies. Future observations of the redshifted 21cm power spectrum as a function of wavelength and angular direction should provide a three-dimensional map of the distribution of neutral hydrogen (Hogan & Rees 1979; Madau, Meiksin & Rees 1997), where redshift supplies the line-of-sight distance. At different redshifts, different signal characteristics are expected, according to the evolution of density fluctuations and the thermal history of the cosmic gas.

Barkana & Loeb (2005a) explored the consequences of the varying baryonic sound speed for the evolution of perturbations on sub-horizon large-scale structure scales (wavevectors  $k = 0.01\text{--}40 \text{ Mpc}^{-1}$ ) in the redshift range  $z = 20\text{--}150$ , where the analysis involves only gravity; they showed that observations of 21cm fluctuations at these redshifts can measure five easily-separated fluctuation modes. In this paper we extend the redshift range back to cosmic recombination, we consider the largest scales (§2) where general relativity and photon fluctuations play a role, and we also study the smallest scales (§3) where gas pressure has an essential effect. This allows us to study the evolution of temperature fluctuations on all scales, and to produce the first accurate predictions at  $k > 100 \text{ Mpc}^{-1}$  of the baryonic density power spectrum and (in §4 & 5) of 21cm fluctuations. We also calculate (§5) a general feature of the 21cm fluctuation power spectrum, i.e., smoothing by the thermal width of the 21cm absorption line. We give our conclusions in §6.

## 2 GROWTH OF LARGE SCALE DENSITY PERTURBATIONS

Up to recombination the baryons and the photons were tightly coupled, and afterwards the baryons were significantly Compton heated down to  $z \lesssim 200$  and retained some memory of this heating at even lower redshifts. Thus, calculations of the growth of perturbations in the baryon density and temperature must take into consideration the evolution of the photon density and temperature fluctuations. The perturbations in the photons themselves (e.g., Ma & Bertschinger 1995) are not significantly affected by the baryon temperature since the photon pressure dominates strongly over the baryonic pressure.

If we define the photon temperature  $T_\gamma$  at each point as the temperature averaged over all photon directions, then dimensionless fluctuations in this temperature ( $\delta_{T_\gamma}$ ) are related to photon density fluctuations ( $\delta_\gamma$ ) by

$$\delta_\gamma = 4\delta_{T_\gamma} . \quad (1)$$

We can derive an equation for the evolution of fluctuations  $\delta_T$  in the gas temperature  $T$  from the first law of thermodynamics [following the derivation by Barkana & Loeb (2005c)]:

$$dQ = \frac{3}{2}k_B dT - k_B T d \log \rho_b , \quad (2)$$

where  $dQ$  is the heating rate per particle and  $\rho_b$  is the baryon density. In the post-recombination era before the formation of galaxies, the only external heating arises from Thomson scattering of the remaining free electrons with CMB photons, resulting in a heating rate per particle

$$\frac{dQ}{dt} = 4 \frac{\sigma_T c}{m_e} k_B (T_\gamma - T) \rho_\gamma x_e(t) , \quad (3)$$

where  $\sigma_T$  is the Thomson scattering cross section,  $\rho_\gamma$  is the photon energy density, and  $x_e(t)$  is the electron fraction out of the total number density of gas particles at time  $t$ . After cosmic recombination,  $x_e(t)$  changes due to the slow recombination rate of the residual ions:

$$\frac{dx_e}{dt} = -\alpha_B(T) x_e^2 (1 + y) \bar{n}_H , \quad (4)$$

where  $\bar{n}_H$  is the mean number density of hydrogen at time  $t$ ,  $y = 0.079$  is the helium to hydrogen number density ratio, and  $\alpha_B(T)$  is the case-B recombination coefficient of hydrogen. We assume that the residual electron fraction is uniform. Fluctuations in  $x_e$  are expected to be very small, since the gas in every region starts out fully ionized and the final  $x_e$  depends on the total accumulated number of recombinations; most recombinations occur early during cosmic recombination, and the recombination rate slows down greatly once most of the gas has recombined, making  $x_e$  insensitive at that point to the gas density and temperature. E.g., since the cosmic mean  $x_e$  declines by only a factor of 1.3 between  $z = 100$  and 20, we estimate that in this redshift range, fluctuations in  $x_e$  are smaller than density fluctuations by a factor of  $\sim 20$ .

Combining equations (2) and (3) we obtain

$$\frac{dT}{dt} = \frac{2}{3} T \frac{d \log \rho_b}{dt} + \frac{x_e(t)}{t_\gamma} \frac{\rho_\gamma}{\bar{\rho}_\gamma} (T_\gamma - T) a^{-4} , \quad (5)$$

where

$$t_\gamma^{-1} \equiv \frac{8}{3} \bar{\rho}_\gamma^0 \frac{\sigma_T c}{m_e} = 8.55 \times 10^{-13} \text{ yr}^{-1} \quad (6)$$

and  $a$  is the scale factor. Thus the evolution of the cosmic mean gas temperature is

$$\frac{d\bar{T}}{dt} = -2H\bar{T} + \frac{x_e(t)}{t_\gamma} (\bar{T}_\gamma - \bar{T}) a^{-4} , \quad (7)$$

where  $\bar{T}_\gamma = [2.725 \text{ K}]/a$  is the mean CMB temperature, and the first-order equation for the perturbation is

$$\frac{d\delta T}{dt} = \frac{2}{3} \frac{d\delta_b}{dt} + \frac{x_e(t)}{t_\gamma} a^{-4} \left\{ \delta_\gamma \left( \frac{\bar{T}_\gamma}{\bar{T}} - 1 \right) + \frac{\bar{T}_\gamma}{\bar{T}} (\delta_{T_\gamma} - \delta_T) \right\} . \quad (8)$$

The first term on the right-hand-side of each of these two equations accounts for adiabatic expansion of the gas, and the remaining terms capture the effect of the thermal exchange with the CMB.

We have numerically calculated the evolution of the perturbations by modifying the CMBFAST code (Seljak & Zaldarriaga 1996) according to these equations for the temperature perturbations (along with other modifications on small scales that are described in the next section). The initial conditions for the temperature at  $z \gtrsim 10000$  are  $\delta_T = \delta_{T_\gamma}$  because of the tight thermal coupling between the gas and the CMB. At lower redshifts, the mechanical coupling weakens but the thermal coupling remains strong, i.e.,

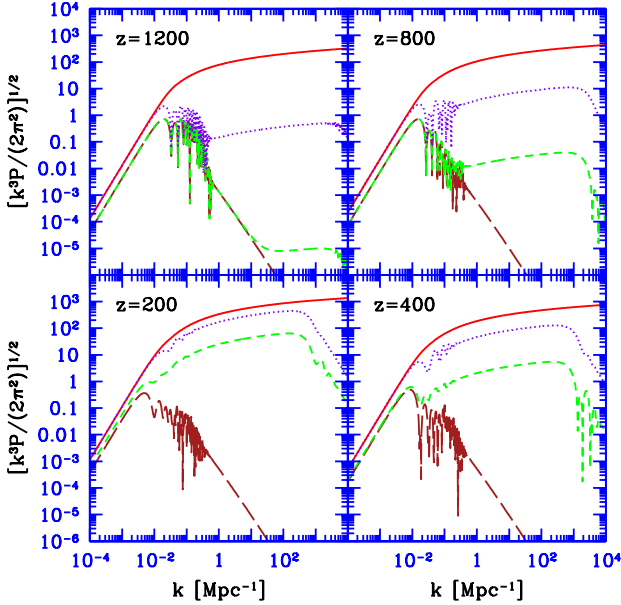


**Figure 1.** Power spectra of density and temperature fluctuations vs. comoving wavenumber, at redshifts 1200, 800, 400, and 200. We consider fluctuations in the CDM density (solid curves), baryon density (dotted curves), baryon temperature (short-dashed curves), and photon temperature (long-dashed curves).

the coefficient of the coupling term in equation (8) remains very large, and it is numerically highly inefficient to solve this equation directly. We instead develop a simple approximation that may be used during this era of thermal tight coupling. First we write the expression for  $d(\delta_T - \delta_{T_\gamma})/dt$  using equation (8) along with the expression for  $d\delta_{T_\gamma}/dt$  as computed by CMBFAST. As long as the thermal coupling is effective, the difference  $\delta_T - \delta_{T_\gamma}$  is very small, i.e.,  $|\delta_T - \delta_{T_\gamma}| \ll |\delta_b|$ , so that the various terms in the expression for  $d(\delta_T - \delta_{T_\gamma})/dt$  must cancel each other nearly completely. Since this expression depends on  $\delta_T$  [see the right-hand side of equation (8)], we simply set  $\delta_T$  to the value that yields  $d(\delta_T - \delta_{T_\gamma})/dt \equiv 0$ . We have checked that using this approximation down to  $z = 900$  affects the power spectra by a fraction of a percent at most.

For the concordance set of cosmological parameters (Spergel et al. 2003), with a scale-invariant primordial power spectrum normalized to  $\sigma_8 = 0.9$  at  $z = 0$ , Figure 1 compares the magnitude of the fluctuations in the CDM and baryon densities, and in the baryon and photon temperatures. For each quantity, the plot shows the dimensionless combination  $[k^3 P(k)/(2\pi^2)]^{1/2}$ , where  $P(k)$  is the corresponding power spectrum of fluctuations. Note that regions where the fluctuations oscillate in sign (as a function of  $k$ ) are difficult to show precisely in such a plot (e.g., the photons and baryons at  $k = 0.01$ – $1 \text{ Mpc}^{-1}$  at  $z = 1200$ , and the baryon temperature at  $k > 1000 \text{ Mpc}^{-1}$  at  $z = 400$ ). Note also that the photon temperature perturbations as shown are simply  $1/4$  of the photon density perturbations [see eq. (1)].

After recombination, two main forces affect the baryon density and temperature fluctuations, namely, the thermal-

ization with the CMB and the gravitational force that attracts the baryons to the dark matter potential wells. As shown in the figure, the density perturbations in all species grow together [except that  $\delta_\gamma = (4/3)\delta_b$ ] on scales where gravity is unopposed, outside the horizon (i.e., at  $k \lesssim 0.01 \text{ Mpc}^{-1}$  at  $z \sim 1000$ ). At  $z = 1200$  the perturbations in the baryon-photon fluid oscillate as acoustic waves on scales of order the sound horizon ( $k \sim 0.01$ ), while smaller-scale perturbations in both the photons and baryons are damped by photon diffusion (Silk damping) and the drag of the diffusing photons on the baryons. Since the initial dark matter density perturbations increase with  $k$ , while the photon perturbations are damped on the smallest scales by photon free streaming, on sufficiently small scales the power spectra of  $\delta_b$  and  $\delta_T$  roughly assume the shape of the dark matter fluctuation  $\delta_{\text{dm}}$  (except for the gas-pressure cutoff at the smallest scales), due to the effect of gravitational attraction on  $\delta_b$  and of the resulting adiabatic expansion on  $\delta_T$ .

This evolution involves two similar physical systems. In each case, a target perturbation  $\delta_0$  is driven toward one perturbation  $\delta_1$ , but this forcing is opposed by coupling to a second perturbation  $\delta_2$ . The values of  $\delta_1$  and  $\delta_2$  are comparable on large scales but  $|\delta_2| \ll |\delta_1|$  on small scales. As long as the coupling is strong,  $\delta_0 \approx \delta_2$  on large scales, while the effect of  $\delta_1$  is apparent in the form of  $\delta_0$  on small scales although the coupling maintains  $|\delta_0| \ll |\delta_1|$ . After the coupling weakens, the perturbation  $\delta_0$  is free to begin rising toward  $\delta_1$ , but this rise occurs only gradually. In the first case,  $\delta_0 = \delta_b$  is driven by gravity toward  $\delta_1 = \delta_{\text{dm}}$ , while mechanical coupling to  $\delta_2 = \delta_\gamma$  is the opposing force. In the second case,  $\delta_0 = \delta_T$  is driven by adiabatic expansion toward  $\delta_1 = \frac{2}{3}\delta_b$ , with resistance provided by thermal coupling to  $\delta_2 = \delta_{T_\gamma}$ . The mechanical coupling ends at  $z \sim 1000$  while the thermal coupling is over by  $z \sim 200$ .

The Figure also shows that the thermal tight-coupling approximation is accurate at the highest redshifts shown, on large scales since  $|\delta_T - \delta_{T_\gamma}| \ll |\delta_{T_\gamma}| < |\delta_b|$ , while on small scales  $\delta_T$  and  $\delta_{T_\gamma}$  are not strongly coupled but each is individually very small compared to  $\delta_b$ . Even at somewhat lower redshifts,  $\delta_b \ll \delta_{\text{dm}}$  and  $\delta_T \ll \delta_b$  on sub-horizon scales. By  $z = 200$  the baryon infall into the dark matter potentials is well advanced and adiabatic expansion is becoming increasingly important in setting the baryon temperature. By this redshift, the photon perturbations are already negligible at  $k \gtrsim 0.01 \text{ Mpc}^{-1}$ , justifying their neglect by Barkana & Loeb (2005c) on these scales.

### 3 GROWTH OF SMALL SCALE DENSITY PERTURBATIONS

On small scales (i.e., at large wavenumbers) the baryon perturbation growth is affected by the pressure of the gas, which affects the dark matter as well since the baryons contribute a small but significant fraction of the total gravitational force. The evolution of sub-horizon linear perturbations is described by two coupled second-order differential equations. The dark matter feels the combined gravity of itself and the baryons:

$$\ddot{\delta}_{\text{dm}} + 2H\dot{\delta}_{\text{dm}} = \frac{3}{2}H_0^2 \frac{\Omega_m}{a^3} (f_b \delta_b + f_{\text{dm}} \delta_{\text{dm}}), \quad (9)$$

where  $\Omega_m$  is the redshift zero matter density as a fraction of the critical density. The baryons feel both gravity and pressure. Prior analyses assumed a spatially uniform baryonic sound speed  $c_s(t)$  (e.g., Ma & Bertschinger 1995), yielding

$$\ddot{\delta}_b + 2H\dot{\delta}_b = \frac{3}{2}H_0^2 \frac{\Omega_m}{a^3} (f_b \delta_b + f_{dm} \delta_{dm}) - \frac{k^2}{a^2} c_s^2 \delta_b, \quad (10)$$

where  $c_s^2 = dp/d\rho$  was calculated from the thermal evolution of a uniform gas undergoing Hubble expansion:

$$c_s^2 \equiv \frac{k_B \bar{T}}{\mu} \left( 1 - \frac{1}{3} \frac{d \log \bar{T}}{d \log a} \right), \quad (11)$$

where  $\mu$  is the mean molecular weight. This also meant that the gas temperature fluctuation was assumed to be proportional throughout space to the density fluctuation, so that

$$\frac{\delta_T}{\delta_b} = \frac{\bar{c}_s^2}{k_B \bar{T} / \mu} - 1. \quad (12)$$

In this paper we instead use the equation of state of an ideal gas to derive a more general equation for the baryons,

$$\ddot{\delta}_b + 2H\dot{\delta}_b = \frac{3}{2}H_0^2 \frac{\Omega_m}{a^3} (f_b \delta_b + f_{dm} \delta_{dm}) - \frac{k^2}{a^2} \frac{k_B \bar{T}}{\mu} (\delta_b + \delta_T). \quad (13)$$

Note that during recombination, we make a similar correction of the baryonic pressure force in the equations of CMB-FAST. In order to solve for the density perturbations, an evolution equation for the fluctuations in the temperature is also required. On sub-horizon scales and at  $z \lesssim 200$  we can neglect the perturbations in the temperature and density of the photons in equation (8), yielding simply

$$\frac{d\delta_T}{dt} = \frac{2}{3} \frac{d\delta_b}{dt} - \frac{x_e(t)}{t_\gamma} a^{-4} \frac{\bar{T}_\gamma}{\bar{T}} \delta_T. \quad (14)$$

Equations (4), (7), (9), (13) and (14) are a closed set of equations describing the evolution of density and temperature perturbations. We note that Bharadwaj & Ali (2004a) derived a similar equation to Eq.(14) but solved it only for the case of a density perturbation that follows the Einstein-de Sitter growing mode  $\delta_b \propto a$  and thus neglected spatial variations in the speed of sound.

Figure 2 shows the power spectra at redshift 20 and 100. As time passes, the power spectrum of the baryons approaches that of the dark matter except for the pressure cutoff, and the baryon temperature fluctuations increase as well. However, even during the era of the formation of the first galaxies ( $z \sim 40$ –20), there is still significant memory in the perturbations of their earlier coupling to the CMB. This is highlighted in Figure 3, which shows the ratios  $\delta_b/\delta_{dm}$  and  $\delta_T/\delta_b$ . In both quantities, the strong oscillations that are apparent at  $z = 400$  are slowly smoothed out toward lower redshifts. At the largest scales, the baryons follow the dark matter density, and  $\delta_T/\delta_b$  evolves from  $1/3$  (the value during tight thermal coupling to the CMB) to  $\sim 2/3$  (from adiabatic expansion). On smaller scales, the two ratios start from values  $\ll 1$  during mechanical/thermal coupling, and increase towards  $\delta_b/\delta_{dm} = 1$  and  $\delta_T/\delta_b = 2/3$ , respectively. The former ratio approaches its asymptotic value earlier, since the baryons decouple from the photons first mechanically and only later thermally. At the smallest scales (below the baryonic Jeans scale), the baryon fluctuation is suppressed at all redshifts due to gas pressure, when the  $k^2$  term in equation (13) dominates. It is clear from this figure

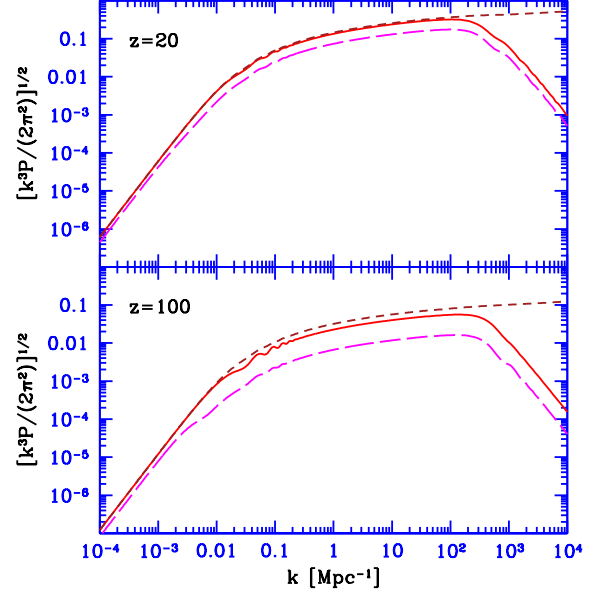


**Figure 2.** Power spectra of density and temperature fluctuations vs. comoving wavenumber, at redshifts 100 and 20. We consider fluctuations in the CDM density (short-dashed curves), baryon density (solid curves), and baryon temperature (long-dashed curves).

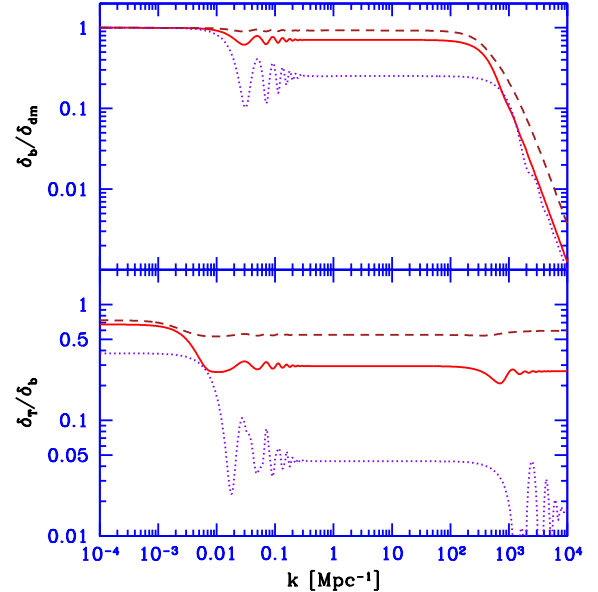


**Figure 3.** Perturbation ratios  $\delta_b/\delta_{dm}$  and  $\delta_T/\delta_b$  vs. comoving wavenumber. We consider  $z = 400$  (dotted curves),  $z = 100$  (solid curves), and  $z = 20$  (dashed curves).

that the traditional assumption of  $\delta_T/\delta_b$  being independent of scale is inaccurate at all redshifts considered here.

Figure 4 shows a detailed comparison between the fluctuation growth described by our improved equation (13) and that given by the traditional equation (10). In the improved calculation, the ratio  $\delta_T/\delta_b$  shows different behaviors on the

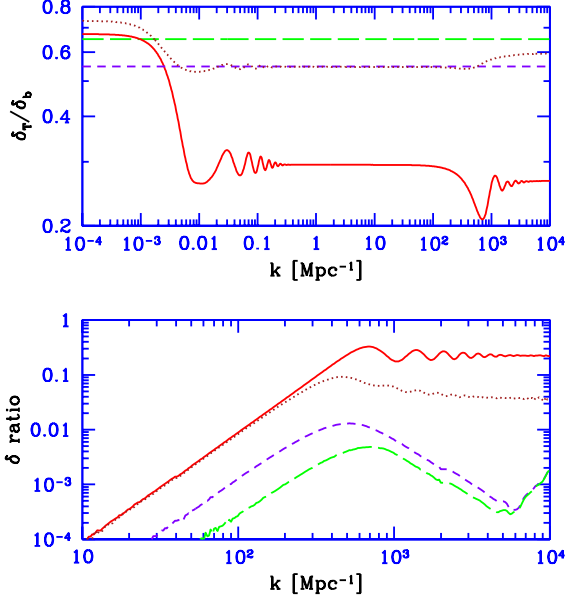


**Figure 4.** Perturbation ratios vs. comoving wavenumber. The upper panel shows the ratio  $\delta_T/\delta_b$ . We consider the improved calculation of equation (13) at  $z = 100$  (solid curve) and  $z = 20$  (dotted curve), compared to the traditional calculation of equation (10) at  $z = 100$  (short-dashed curve) and  $z = 20$  (long-dashed curve). The lower panel shows the ratio between the perturbations in the improved calculation and those in the traditional (mean  $c_s$ ) calculation. We show the ratio of  $\delta_b$  values at  $z = 100$  (solid curve) and  $z = 20$  (dotted curve). Also shown is the ratio of  $\delta_{dm}$  values at  $z = 100$  (short-dashed curve) and  $z = 20$  (long-dashed curve). Note that the displayed  $\delta_{dm}$  ratios have been smoothed at  $k \gtrsim 3000 \text{ Mpc}^{-1}$  to suppress noise due to limited numerical precision in CMBFAST.

scale of the horizon, the photon acoustic oscillations, and on smaller scales. Although the ratio is roughly constant over some ranges of scales, its value differs from that of the traditional calculation. The improved calculation changes the temperature fluctuations on all scales by  $\gtrsim 10\%$  at  $z = 20$ , and by much more at  $z = 100$ . Note that at the lower redshift,  $\delta_T/\delta_b$  at the small- $k$  end is higher than the adiabatic value of  $2/3$ , since when  $\bar{T}$  falls significantly below  $\bar{T}_\gamma$  the thermal coupling tends to heat the gas more strongly in regions with a higher photon density [see the  $\delta_\gamma$  term in eq. (8)].

We also present in the lower panel of this Figure the ratio between the fluctuations in the improved calculation and those in the traditional calculation. Although the improved calculation has only a small effect on the dark matter density ( $\lesssim 1\%$ ) and a similarly small effect on the baryon density at  $k < 100 \text{ Mpc}^{-1}$ , on smaller scales the baryon fluctuations are substantially affected. The baryon fluctuations are changed by up to 30% at  $z = 100$  and 10% at  $z = 20$ . Thus, accurate initial conditions for models and simulations of the formation of the first galaxies require a full calculation of the evolution of baryon density and temperature fluctuations along with the dark matter.

#### 4 21cm FLUCTUATIONS AND THE SPIN TEMPERATURE

Quantitative calculations of 21cm absorption begin with the spin temperature  $T_s$ , defined through the ratio between the number densities of hydrogen atoms,

$$\frac{n_1}{n_0} = \frac{g_1}{g_0} e^{-T_\star/T_s}, \quad (15)$$

where subscripts 1 and 0 correspond to the excited and ground state levels of the 21cm transition,  $(g_1/g_0) = 3$  is the ratio of the spin degeneracy factors of the levels, and  $T_\star = 0.0682\text{K}$  corresponds to the energy difference between the levels. The 21cm spin temperature is on the one hand radiatively coupled to the CMB temperature, and on the other hand coupled to the kinetic gas temperature  $T$  through collisions (Allison & Dalgarno 1969) or the absorption of Ly $\alpha$  photons (Wouthuysen 1952; Field 1958). For the concordance set of cosmological parameters (Spergel et al. 2003), the mean brightness temperature on the sky at redshift  $z$  (relative to the CMB itself) is (Madau, Meiksin & Rees 1997)

$$T_b = 28 \text{ mK} \left( \frac{1+z}{10} \right)^{1/2} \left( \frac{T_s - T_\gamma}{T_s} \right) \bar{x}_{\text{HI}}, \quad (16)$$

where  $\bar{x}_{\text{HI}}$  is the mean neutral fraction of hydrogen.

In general, fluctuations in  $T_b$  can be sourced by fluctuations in gas density, temperature, neutral fraction, radial velocity gradient, and Ly $\alpha$  flux from galaxies. In this paper we consider the era before the formation of a significant galaxy population, so that  $\bar{x}_{\text{HI}} = 1$  and there is no Ly $\alpha$  flux. The velocity gradient term (Sobolev 1960) is in Fourier space (Kaiser 1987; Bharadwaj & Ali 2004b)  $\tilde{\delta}_{d_r v_r} = -\mu^2 \tilde{\delta}_b / H$ , where  $d_r v_r$  is the line-of-sight gradient of the line-of-sight gas velocity, and  $\mu = \cos \theta_k$  in terms of the angle  $\theta_k$  of  $\mathbf{k}$  with respect to the line of sight. We can therefore write the fluctuation in the brightness temperature  $T_b$  as (Barkana & Loeb 2005a)

$$\tilde{\delta}_{T_b}(\mathbf{k}, t) = \mu^2 \tilde{\delta}_b(\mathbf{k}) H^{-1} + \beta \tilde{\delta}_b(\mathbf{k}) + \beta_T \tilde{\delta}_T(\mathbf{k}), \quad (17)$$

where we have defined time-dependent coefficients  $\beta$  and  $\beta_T$  [combining the relevant explicit terms from eq. (2) of Barkana & Loeb (2005a)]. Before the first galaxies, these coefficients depended only on the cosmic mean hydrogen density  $\bar{n}_H$  and the temperatures  $\bar{T}_\gamma$  and  $\bar{T}$ .

Figure 5 shows the redshift evolution of the various mean temperatures and the coefficients  $\beta$  and  $\beta_T$ . As discussed above, after recombination the small residual fraction of free electrons coupled the temperature of the baryons to that of the photons. Thus, after recombination the levels of the hyperfine transition were at thermal equilibrium with the CMB temperature as well as the temperature of the gas, i.e.,  $T_s \sim T \sim T_\gamma$ , and no signal is expected. At  $z \lesssim 200$  the gas temperature dropped below the CMB temperature [ $T_\gamma \propto (1+z)$ ], eventually dropping adiabatically [ $T \propto (1+z)^2$ ]. Atomic collisions in the still-dense cosmic gas kept  $T_s$  below  $T_\gamma$  thus allowing the gas to absorb at 21cm against the CMB (Loeb & Zaldarriaga 2004). The detection of 21cm fluctuations would uncover the thermal history of the epoch prior to the end of cosmic reionization, and measure the growth of the baryon density and temperature perturbations.

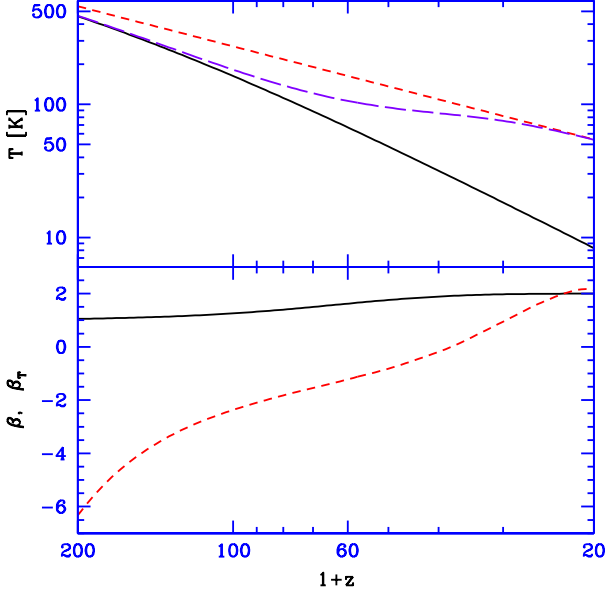


**Figure 5.** The upper panel plots mean temperatures vs. redshift. We consider  $T$  (solid curve),  $T_\gamma$  (short-dashed curve), and the 21cm spin temperature  $T_s$  (long-dashed curve). The lower panel shows the 21cm coefficients  $\beta$  (solid curve) and  $\beta_T$  (dashed curve) vs. redshift.

## 5 THERMAL SMOOTHING OF THE 21cm POWER SPECTRUM

About 1% of the 21cm photons that propagate through the atomic medium suffer scattering by hydrogen. Scattering at a given observed wavelength of  $21(1+z)$  cm does not occur sharply at redshift  $z$ , but rather is distributed over a narrow interval about  $z$ . This is due to the finite width of the 21cm absorption line, set by a combination of the natural linewidth and the thermal motions of the hydrogen atoms. The resulting cutoff in the power spectrum was estimated crudely by Barkana & Loeb (2005b), but here we calculate it precisely along with its angular dependence. Note that this cutoff arises from the use of an absorption line as a probe, and is a separate effect from the Jeans smoothing of the density discussed above.

We can obtain the observed 21cm fluctuation by starting with the previous, unsmoothed value and smoothing it along the line of sight. The cross-section for scattering has a thermal width  $\Delta\nu_D$  given by

$$\Delta\nu_D = \sqrt{\frac{2k_B T}{m_H}} \frac{\nu_{21}}{c}, \quad (18)$$

where  $\nu_{21}$  is the frequency of the center of the line. The line profile is given by the normalized Voigt profile function  $\phi$ , which represents a convolution between the natural broadening and the thermal broadening, and is given by

$$\phi(\xi) = \frac{u}{\pi^{3/2}} \int_{-\infty}^{\infty} d\eta \frac{e^{-\eta^2}}{(\xi - \eta)^2 + u^2}, \quad (19)$$

where  $\xi = (\nu - \nu_{21})/\Delta\nu_D$  and  $u = A_{10}/(4\pi\Delta\nu_D)$  are the dimensionless Voigt parameters, and  $A_{10} = 2.87 \times 10^{-15} \text{ s}^{-1}$  is the Einstein spontaneous emission coefficient for the 21cm

transition. The line profile smoothes the absorption along the line-of-sight direction (comoving coordinate  $z_c$ ), while no such smoothing occurs in the perpendicular directions ( $x_c$  and  $y_c$ ). It is convenient to express the result as a smoothing with a three-dimensional window function:

$$\delta_{T_b}^W(\mathbf{r}_0) = \int \delta_{T_b}(\mathbf{r} - \mathbf{r}_0) W(\mathbf{r}) d^3\mathbf{r}. \quad (20)$$

In calculating the smoothing we translate frequency to comoving coordinate  $z_c$  using the homogeneous relation  $(\nu_{21}/\nu) - 1 = aH z_c/c$ , neglecting higher-order corrections. The resulting window function is

$$W(\mathbf{r}) = \frac{1}{\sqrt{2}R_T} \phi(\xi(z_c)) \delta_D(x_c) \delta_D(y_c), \quad (21)$$

where  $\delta_D$  is a one-dimensional Dirac delta function and we have defined

$$R_T = \frac{1}{aH} \sqrt{\frac{k_B T}{m_H}} = 0.768 \sqrt{\frac{T}{\text{K}}} \left( \frac{\Omega_m h^2}{0.14} \right)^{-\frac{1}{2}} \left( \frac{1+z}{10} \right)^{-\frac{1}{2}} \text{ kpc}, \quad (22)$$

where the second expression for  $R_T$  is valid in an Einstein de-Sitter universe (i.e., is accurate at  $z \sim 3-150$ ). The resulting power spectrum  $P_{T_b}$  of temperature brightness fluctuations is related to its unsmoothed value  $P_{T_b}^0$  by

$$P_{T_b} = P_{T_b}^0 |\tilde{W}_k|^2. \quad (23)$$

The Fourier transform  $\tilde{W}_k$  of the window function  $W$  is easily derived to be

$$\tilde{W}_k = e^{-\sqrt{2}k\mu u R_T} e^{-\frac{1}{2}(k\mu R_T)^2}, \quad (24)$$

where  $\mu = \cos\theta_k$  in terms of the angle  $\theta_k$  of  $\mathbf{k}$  with respect to the line of sight. This simple factorization of the Fourier transform is expected, since the line profile was constructed by convolving a Lorentzian and a Gaussian, and so the compound Fourier transform is simply the product of the individual transforms.

The smoothing effect is characterized by two parameters,  $R_T$  and  $u$ . The parameter  $u$  measures the relative importance of the natural compared to the thermal line width, and its extremely low value,  $u = 3.74 \times 10^{-19} (T/\text{K})^{-1/2}$ , indicates that the natural width is in practice negligible. We note that collisional broadening is expected to dominate over the natural broadening, but even collisions with other atoms, which contribute the highest collision rate, produce broadening that is greater than the natural width by only a few orders of magnitude, and this is still negligible relative to the thermal broadening. Thus, the only significant term is the Gaussian term in  $\tilde{W}_k$ , which cuts off the 21cm power spectrum at small scales, regardless of the physical source of the 21cm fluctuations. The cutoff drops the power spectrum by a factor of  $e$  at a wavevector  $k = 1/(\mu R_T)$ , where, e.g.,  $R_T = 3.1 \text{ kpc}$  at  $z = 100$  and  $1.6 \text{ kpc}$  at  $z = 20$ . Larger cutoff scales are possible if the intergalactic medium is later heated by galactic radiation; e.g.,  $T = 10^3 \text{ K}$  at  $z = 20$  implies  $R_T = 17 \text{ kpc}$ .

Since the unsmoothed power spectrum is a polynomial in  $\mu^2$  (Barkana & Loeb 2005c), we find

$$P_{T_b} = [\mu^4 P_{\mu^4}(k) + \mu^2 P_{\mu^2}(k) + P_{\mu^0}(k)] e^{-(k\mu R_T)^2}. \quad (25)$$

At each  $k$ , the power spectrum at four different values of  $\mu$  suffices to measure separately the three power spectra  $P_{\mu^4}$ ,



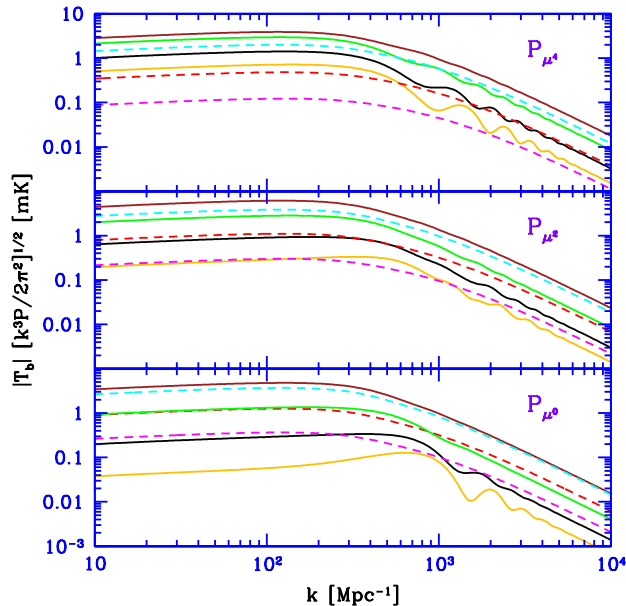


**Figure 6.** Power spectra of 21cm brightness fluctuations versus comoving wavenumber. We show the three power spectra that are separately observable,  $P_{\mu^4}$  (upper panel),  $P_{\mu^2}$  (middle panel), and  $P_{\mu^0}$  (lower panel). In each case we show redshifts 200, 150, 100, 50 (solid curves, from bottom to top), 35, 25, and 20 (dashed curves, from top to bottom).

$P_{\mu^2}$ , and  $P_{\mu^0}$ , and the value of  $R_T$ . If many values of  $\mu$  are measured over a range of different  $k$ 's (including sufficiently large  $k$  values), then the thermal cutoff scale  $R_T$  can be measured accurately, directly yielding a combination of  $T$  and  $H$ . Comparison with the three power spectra can be used to check for self-consistency and to measure cosmological parameters, since the power spectra also depend on  $T$  [through  $\beta$  and  $\beta_T$  in eq. (17)] and on the parameters (through  $H$  and the growth of the perturbations).

Barkana & Loeb (2005a) showed that it would be difficult to measure 21cm fluctuations on the largest scales ( $k \lesssim 0.01 \text{ Mpc}^{-1}$ ), since they are small and angular projections do not help. Barkana & Loeb (2005c) calculated the 21cm fluctuations on intermediate large-scale structure scales, so here we focus on the predicted magnitude of small-scale fluctuations at  $k > 10 \text{ Mpc}^{-1}$ . Figure 6 tracks the three 21cm power spectra from redshift 200 to 20. Each power spectrum rises to a maximum fluctuation level of  $\sim 5 \text{ mK}$  at  $z = 50$ , and subsequently drops due to the reduced collisional coupling of the 21cm transition to the gas temperature. Small-scale oscillations are visible at  $z > 100$ , with a smoother cutoff at lower redshifts. The additional thermal smoothing (not shown in the figure) occurs at a scale where the unsmoothed signal is  $\sim 0.1\text{--}1 \text{ mK}$ .

## 6 CONCLUSIONS

We have computed the linear growth of fluctuations over the entire range of scales from those outside the horizon down to the scales that are affected by baryonic pressure. We have shown that the baryonic sound speed varies spatially,

so that the temperature and density fluctuations must be tracked separately. At large wavenumbers ( $k \gtrsim 100 \text{ Mpc}^{-1}$ ) the growth of baryon density fluctuations is changed significantly by the inhomogeneous sound speed, by up to 30% at  $z = 100$  and 10% at  $z = 20$ . The effect on the dark matter evolution is much more modest since the baryons contribute only a small fraction of the total gravitational force felt by the dark matter.

After cosmic recombination, the gas decouples mechanically from the photons, but remains thermally coupled down to  $z \sim 200$ . Starting from very low values on sub-horizon scales, the baryon density perturbations gradually approach those in the dark matter, and (somewhat later) the temperature perturbations approach the value expected for an adiabatic gas. An aftermath of cosmic recombination is the signature of the large-scale acoustic oscillations of the baryon-photon fluid at  $k \sim 0.01\text{--}0.2 \text{ Mpc}^{-1}$ . This remnant is most apparent in the baryon density power spectrum but it diminishes with time. At small scales, the cutoff due to gas pressure is apparent at all redshifts at  $k \gtrsim 10^3 \text{ Mpc}^{-1}$ , and can be measured directly from 21cm fluctuations which reach a magnitude higher than 1 mK in the redshift range  $z = 100\text{--}25$ .

In addition we have calculated the smoothing of the 21cm power spectrum due to the finite width of the 21cm line. This effect is dominated by the thermal motions of the scattering hydrogen atoms, and is always present regardless of the source of the 21cm fluctuations. This effect produces an anisotropic Gaussian cutoff of the power spectrum at small scales,  $k \gtrsim 1 \text{ kpc}^{-1}$ , similar to the characteristic wavenumber of suppression due to the baryonic pressure. Measuring the thermal smoothing along the line of sight requires a high resolution in frequency, e.g.,  $\sim 25 \text{ Hz}$  at  $z = 50$  compared to the redshifted 21cm frequency of 28 MHz.

We conclude that accurate initial conditions for analytical models and numerical simulations of galaxy formation require a full calculation of the evolution of perturbations that includes the spatial fluctuations in the baryonic sound speed. At high redshift the gas temperature fluctuations are still recovering from their thermal coupling to the photons and are quite small at sub-horizon scales; thus, our improved calculation is particularly important for simulations of the formation of the first galaxies.

## ACKNOWLEDGMENTS

We acknowledge support by NSF grant AST-0204514 and Israel Science Foundation grant 28/02/01.

## REFERENCES

- Allison, A. C., & Dalgarno, A. 1969, *ApJ*, 158, 423
- Barkana, R., & Loeb, A. 2001, *Phys. Rep.*, 349, 125
- Barkana, R., & Loeb, A. 2005a, *ApJ*, submitted [astro-ph/0409572]
- Barkana, R., & Loeb, A. 2005b, *ApJ*, accepted [astro-ph/0410129]
- Barkana, R., & Loeb, A. 2005c, *ApJ*, submitted [astro-ph/0502083]
- Becker, R. H., et al. 2001, *ApJ*, 122, 2850

- Bennett, C. L., et al. 1996, *ApJ*, Lett. 464, 1
- Bharadwaj, S., & Ali, S. S. 2004a, *MNRAS*, 352, 142
- Bharadwaj, S., & Ali, S. S. 2004b, *MNRAS*, 356, 1519
- Ciardi, B. & Madau, P. 2003, *ApJ*, 596, 1
- Fan, X., et al. 2002, *ApJ*, 123, 1247
- Field, G. B. 1958 *Proc. IRE* 46, 240
- Gnedin, N. Y. & Hui, L. 2004, *MNRAS*, 296
- Hogan, C. J., & Rees, M. J. 1979, *MNRAS* 188, 791
- Kaiser, N. 1987, *MNRAS*, 227, 1
- Kogut, A., et al. 2003, *ApJ*, 148, 161
- Loeb, A., & Zaldarriaga, A. 2004, *PRL*, 92, 211301
- Ma, C. & Bertschinger, E. 1995, *ApJ*, 455, 7
- Madau, P., Meiksin, A. & Rees, M. J. 1997, *ApJ*, 475, 429
- Peebles, P. J. E. 1980, *The large-scale structure of the universe*, Princeton U. Press: Princeton
- Peebles, P. J. E. 1993, *Principles of physical cosmology*, Princeton U. Press: Princeton
- Press, W. H., & Schechter, P. 1974, *ApJ*, 187, 425
- U., Seljak, & M., Zaldarriaga 1996, *ApJ*, 469, 437; see <http://www.cmbfast.org>
- Sobolev, V. V., 1960 *Moving Envelopes of Stars*, Cambridge: Harvard University Press
- Spergel, D. N., et al. 2003, *ApJ*, 148, 175
- Wouthuysen, S. A. 1952, *ApJ*, 57, 31
- Yamamoto, K., Sugiyama, N., & Sato, H. 1997, *PRD*, 56, 7566
- Yamamoto, K., Sugiyama, N., & Sato, H. 1998, *ApJ*, 501, 442

This paper has been typeset from a  $\text{\LaTeX}$  file prepared by the author.